Molecular Therapy
Methods & Clinical Development
Original Article

Enhanced Production of Exosome-Associated AAV by Overexpression of the Tetraspanin CD9

Lara Timantra Schiller,[1,3] Nicolás Lemus-Diaz,[1,3] Rafael Rinaldi Ferreira,[1] Kai Oliver Böker,[1,2] and Jens Gruber[1]

[1]Junior Research Group Medical RNA Biology, German Primate Center, Leibniz Institute for Primate Research, Kellnerweg 4, 37077 Göttingen, Germany; [2]Department for Trauma Surgery, Orthopaedics and Plastic Surgery, University Medical Center Göttingen, Robert-Koch Straße 40, 37075 Göttingen, Germany

Research on cell-free vesicles revealed a multitude of characteristics, in particular of microvesicles and exosomes, that range from their potential as biomarkers to a function in horizontal transfer of genetic information from cell to cell and also include supportive functions in viral infection. Exosome-associated adeno-associated viruses (exo-AAVs) are of particular interest for the past couple of years, because they introduced a new source of highly potent recombinant AAVs with improved features, including accelerated transduction rates and more efficient immune escape. However, key factors like the mode of action, efficiency of production, or engineering of exo-AAVs remain elusive to a large extent. Here, we used the established system of CD9 overexpression to boost the exosome output of AAV producing HEK-AAV cells. The CD9-powered high-exosome environment was established during exo-AAV1 production, and we could demonstrate that the yield of exo-AAVs dramatically increased when compared to standard exo-AAVs. Furthermore, we report that exo-AAV-CD9$_{GFP}$ was more efficient in transduction of cells in the same titer ranges as standard exo-AAVs. Our results provide a technological approach for the generation of exo-AAVs with superior performance.

INTRODUCTION

The fundamental principle of gene therapy requires the introduction of exogenous genetic material into the cells to modify, replace, or modulate specific gene functions.[1] To this purpose, viral vectors represent the most promising and useful therapeutic vehicles. Although virus production is well established and widespread for primary and applied research, new methods to improve the quantity, quality, efficacy, and safety are still required to close the gap from research findings to therapeutic products. Therefore, the generation of scalable cell culture processes and optimization of vector yield and quality could improve enormously the future of gene therapy.

Among the viral vectors, adeno-associated viruses (AAVs) are extensively used and hold promise to be the preferred delivery tool in gene therapy. This is due to their non-pathogenic potential, mild immune response,[2] and rare integrative features.[3] Several clinical trials and the first approved virus-based gene therapy on the market have shown their flexibility and potential as therapeutic tools.[4,5] Depending on the serotype, AAVs retain mainly in the packaging cell line or are secreted into the media, indicating that different purification protocols are required.[6] The standard harvesting procedure requires cell lysis and virus separation from cell components by gradient centrifugation or chromatographical methods.[7–9]

During the past decade, exosomes have emerged as novel cell-to-cell communication mediators. Exosomes are vesicles of 30–100 nm in diameter, which are secreted into the extracellular space and work as message carriers of nucleic acids and proteins.[10–13] Although molecular mechanisms of exosome biology are still under investigation, these small vesicles are discussed to be a powerful novel gene delivery tool.

Recent findings from various studies have brought AAVs and exosomes in new context. In 2012, Maguire et al.[14] reported that an AAV population interacts with extracellular vesicles and has a better functional readout than their vesicle-free counterpart. For instance, exosome-associated AAVs (exo-AAV) of AAV1 and AAV2 are more efficient than the corresponding exosome-free standard AAVs in cell culture.[14]

Although the immune response to AAVs is mild, neutralizing antibodies are still a drawback for AAV vectors, and these antibodies are found in several pre-clinical animal models[15] and human subjects with a prevalence of 59.5% of antibodies against AAV1.[16] Surprisingly, exo-AAVs circumvent this issue by increasing resistance against anti-AAV antibodies by shielding the AAV vectors.[14,17]

Exo-AAVs can pass more efficiently through biological barriers, such as the blood-brain barrier[18] or the inner limiting membrane of the retina, after systemic or intravitreal injection,[19] respectively, and show a higher transduction efficiency compared to standard AAVs. For instance, exo-AAV1 can efficiently transduce outer hair cells,[20] exo-AAV9 outperforms standard AAV9 in CNS, and

Received 11 November 2017; accepted 23 March 2018;
https://doi.org/10.1016/j.omtm.2018.03.008.

[3]These authors contributed equally to this work.

Correspondence: Jens Gruber, Junior Research Group Medical RNA Biology, Deutsches Primatenzentrum GmbH, Leibniz Institute for Primate Research, Kellnerweg 4, 37077 Göttingen, Germany.
E-mail: jgruber@dpz.eu

exo-AAV8 requires a lower titer to achieve similar transductions efficiency compared to free AAV8.[18] Additionally, exosomes can be pseudotyped for targeted delivery of small interfering RNA (siRNA), proteins, or AAVs by using viral glycoproteins during exosome production, increasing the repertoire of target specificity, and promising a broader range of applications for extracellular vesicles.[14,17]

As for other tools of gene therapy, the manufacturing and production of exo-AAVs require intensive development and optimization to fulfill future pharmaceutical and good manufacturing practice (GMP) requirements. Recently, we reported that the tetraspanin CD9, a well-known exosome marker,[21] increases exosome production in several cell lines and reduces the overall size of extracellular vesicles.[22] We believe that CD9 has a stabilizing effect on membrane microdomains and that it can be used as an agent to manufacture better exosomes for gene therapy.

Here, as a proof of principle, we demonstrate that $CD9_{GFP}$ overexpression (1) boosts exosome release of AAV producer cells, (2) promotes the production of more efficient exo-AAVs, and (3) increases the amount of exosome-associated AAVs. We suggest that using $CD9_{GFP}$ overexpression in producer cell lines improves exo-AAV harvesting and future manufacturing.

RESULTS

Standard AAV1 and exo-AAV1 Production in Wild-Type and CD9-Overexpressing Cells

To evaluate the impact of $CD9_{GFP}$ overexpression in exo-AAV production, we used the standard HEK-AAV producer cell line and compared it with $CD9_{GFP}$-overexpressing cells. We generated HEK-AAV cells expressing $CD9_{GFP}$ using lentiviral transduction (LV-$CD9_{GFP}$-VSV-G) and tracked the expression by fluorescence-activated cell sorting (FACS) analysis to quantify the percentage of transgene-expressing cells ($CD9_{GFP}^{+}$; Figure 1A). The $CD9_{GFP}$ protein was predominantly membrane localized (Figure 1B).

For AAV production, we used HEK-AAV cells that expressed CD9 in at least 80% of the cells according to GFP expression in FACS analysis (Figure 1). Because selection with antibiotics can change the fundamental characteristics for AAV production, we transduced HEK-AAV cells for each independent biological replicate. HEK-AAV cells of passage five were transduced with LVs and considered for rAAV production with a maximum passage of eight. Recombinant AAV2/1-CAG-GFPs were produced in wild-type and $CD9_{GFP}$-overexpressing HEK-AAV cells by double transfection of the helper plasmid pDP1rs (AAV1) and the expression plasmid pAAV-CAG-GFP (gene cassette flanked by inverted terminal repeats [ITRs] of AAV2).

Standard AAVs were harvested from the cell lysate and purified by an iodixanol density gradient, dialyzed, and concentrated. In contrast, exo-AAVs were purified by differential centrifugation of the conditioned media to separate exosomes (30–100 nm) from more prominent vesicles (Figure 1A). The abundance of exosomes in the 20,000 × *g* and 100,000 × *g* pellets was confirmed by western blot detection of three exosomal marker proteins, i.e., hAlix, CD63, and CD9 (Figure 1C). Anti-GFP detected the GFP expressed from the pAAV and the fusion protein of $CD9_{GFP}$. We utilized standard AAV1 and polyethylene glycol (PEG)-precipitated vesicles of HEK-AAV cells as controls.

$CD9_{GFP}$ Overexpression Boosts Exosome Release

Recently we reported that $CD9_{GFP}$ overexpression increases the overall exosome production.[23] Therefore, we purified vesicles by centrifugation using PEG precipitation. Using nanoparticle tracking analysis (NTA), we measured the concentration and size distribution of extracellular vesicles.

Here, we demonstrate the same finding for $CD9_{GFP}$-overexpressing HEK-AAV cells, which released 3.75 times more exosomes (30–100 nm) to the media. Additionally, the cells released a generally increased number of vesicles with a reduced size (Figures 2A–2C).

To test whether this affirmation is reproducible for the exo-AAV purification protocol, we collected and separated the vesicles according to the exo-AAV harvesting protocol with differential centrifugation (20,000 × *g* and 100,000 × *g*) and analyzed the samples by NTA (Figure 2D). Additionally, extracellular vesicles from the conditioned media and remaining supernatant were harvested via PEG precipitation.

The fractions from the exo-AAV harvesting protocol showed a similar increase of exosome concentration for the overexpressing cells with a disproportionately high increase of exosomes in the 100,000 × *g* pellet. To determine the quality of the exosome purification, we examined the particle size distribution of the 20,000 × *g* and 100,000 × *g* pellets and the remaining supernatant. The 100,000 × *g* fraction contained mainly exosomes, whereas the 20,000 × *g* fraction and the supernatant included more prominent, larger, and less homogeneous vesicles (Figure 2E). These results indicate that $CD9_{GFP}$ overexpression increased the overall exosome content independent of the purification protocol and that the exo-AAV protocol is both reproducible and useful for exosome purification.

$CD9_{GFP}$ Overexpression Yields More Efficient exo-AAVs

After setting a comparable standard of exo-AAV purification (wild-type versus $CD9_{GFP}$ cells) and confirming that $CD9_{GFP}$ overexpression increases the exosome yield, we elucidated whether an exosome increment in $CD9_{GFP}^{+}$ cells improves the exo-AAV yield and functionality.

To examine this, we determined the transducing units, defined as the number of viral particles that are capable of transducing cells, by measuring the GFP expression of transduced cells. We quantified the vector genomes, the commonly given genomic titer, by real-time qPCR (Figure 3A).

We observed no significant difference for the genomic titers between wild-type and $CD9_{GFP}$-producing cells, neither in harvested media

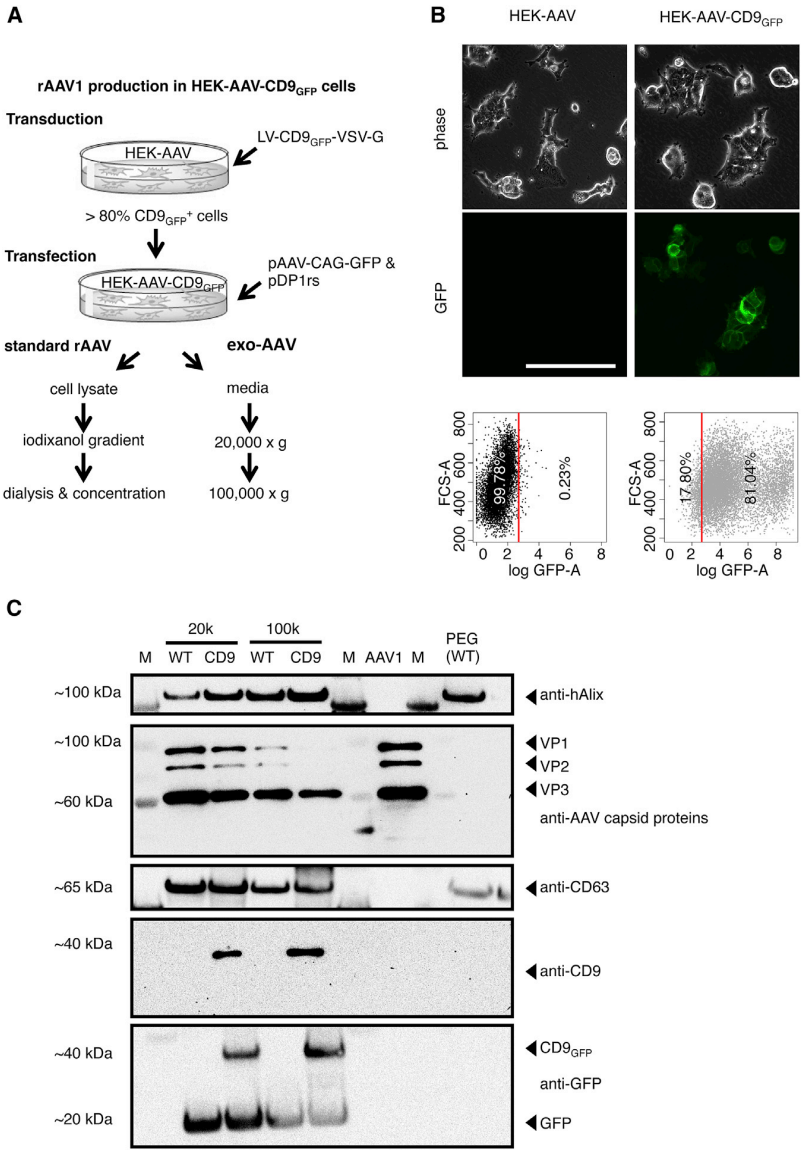

Figure 1. Overview of HEK-AAV-CD9$_{GFP}$ Cell Production with Standard and exo-AAV Harvest

(A) HEK-AAV cells were transduced with LV-CD9$_{GFP}$-VSV-G to gain stable CD9$_{GFP}$-overexpressing cells. Cells were used for AAV production when FACS analysis determined more than 80% CD9$_{GFP}^{+}$ cells. AAV production requires the transfection of pDP1rs, coding for the serotype, and pAAV-CAG-GFP for the gene that is incorporated in the virus. For standard AAV production, cells were lysed, and AAVs were purified by iodixanol density gradient centrifugation, followed by dialysis and concentration. For exo-AAV harvest, the media was successive centrifuged and the pellets of the 20,000 × *g* and 100,000 × *g* centrifugation resuspended in DMEM. (B) FACS and fluorescence-micrographs of WT and recombinant HEK-AAV cells 72 hr after transduction are shown. Dot plots reflect for HEK-AAV-CD9$_{GFP}$ 81% of CD9$_{GFP}^{+}$ cells, which is visualized in micrographs, showing membrane localization of CD9$_{GFP}$. The red line indicates the GFP intensity of two SDs from the mean of the WT measurement, over which cells were considered as CD9$_{GFP}^{+}$. The scale bar represents 200 μm. (C) Western blot detection of exosomal markers (hAlix, CD63, and CD9), AAV capsid proteins, and GFP in 20,000 × *g* and 100,000 × *g* pellets of exo-AAV1 production in wild-type HEK-AAV (WT) and HEK-AAV-CD9$_{GFP}$ (CD9) cells is shown. Standard AAV1 and PEG-precipitated vesicles of HEK-AAV cells as controls are shown. M, marker.

nor on any of the exo-AAV purification steps (Figure 3B). Calculating the total yield of AAVs per cell culture plate (Table 1), we harvested by standard AAVs isolation from the crude lysate two magnitudes more AAVs than with the 100,000 × *g* centrifugation, which was only a minor proportion of the total vector genomes measured in the media.

For the functional titer, we transduced HEK cells with a serial dilution of the virus, analyzed them for GFP expression, and calculated the transducing units for AAV1 conditioned media and 100,000 × *g* exo-AAV1 (Figures 3C and S1). Plotting the transducing units versus vector genomes indicates that CD9$_{GFP}$-derived exo-AAV1 has a higher efficiency because the slope of the linear regression line for AAVs from CD9$_{GFP}$-overexpressing cells is higher than from wild-type cells. Inferring then, exo-AAV1-CD9$_{GFP}$ will lead to more transduced cells compared with exo-AAV1 of the same genomic titer. This behavior was consistent with three independent biological replicates, with exo-AAV1-CD9$_{GFP}$ being 26% ± 4.9% (mean ± SD) more efficient.

The virus-containing medium showed small but significant (7% vector genome [vg]/transducing unit [TU]) differences between CD9$_{GFP}$ and wild-type cells (Table 2; Figure S1). This is consistent with the fact that the medium contains a mixture of free AAVs and exo-AAVs. To exclude that the protein transfer of CD9$_{GFP}$ embedded in the exosomes from the overexpressing cells falsified the determination of transducing units, we transduced in a control experiment HEK cells with 100,000 × *g* pelleted vesicles from such cells. Flow cytometry analysis did indicate no CD9$_{GFP}^{+}$ cells (Figure S2).

Summing up, CD9$_{GFP}$-overexpressing cells produced the same amount of vector genomes, but these viruses, in particular the 100,000 × *g* pelleted (exo-AAVs) are on average 26% ± 4.9% (mean ± SD) more efficient than the ones harvested from wild-type cells.

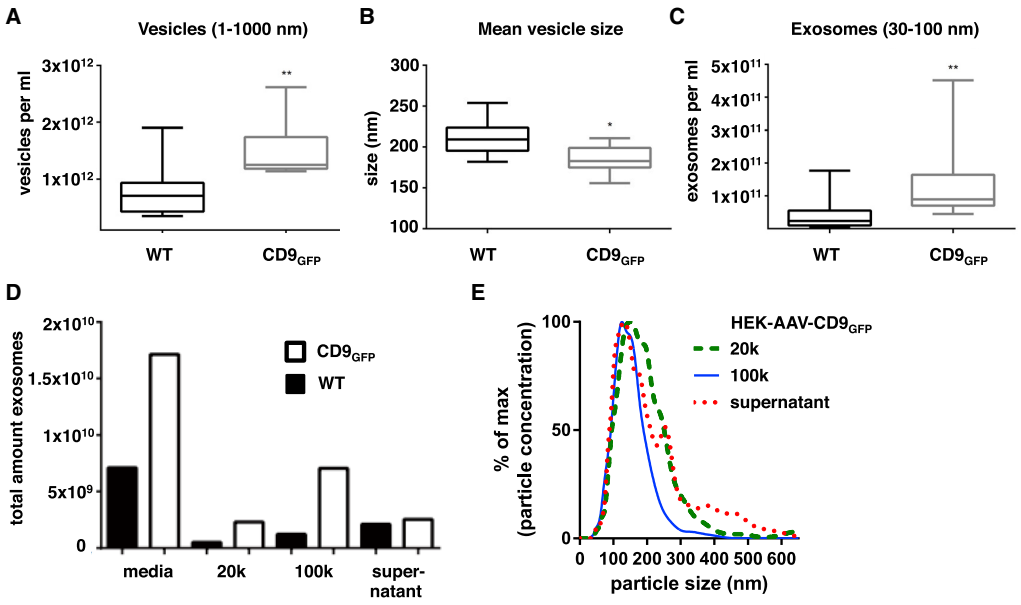

Figure 2. Characterization of Vesicle Content in Media and during exo-AAV Harvesting Procedure

To mimic exo-AAV production conditions, cells were transfected with the pAAV-CAG-GFP. (A–C) Nanoparticle tracking analysis of the cell culture media determined a significantly higher concentration of vesicles with reduced size and an increase in exosome concentration. Biological triplicates were measured in triplicates and the data analyzed by D'Agostino-Pearson test for Gaussian distribution. Normally distributed data were analyzed for significant difference via unpaired t test (B), and non-normal distributed data were analyzed by Mann-Whitney test (A and C). *$p < 0.05$; **$p < 0.01$; error bars indicate the SD. (D) For $CD9_{GFP}$-overexpressing cells, the number of exosomes was higher in each step. It also showed that most exosomes were pelleted at 100,000 centrifugation. (E) Exemplary density plot of vesicle distribution is shown. $CD9_{GFP}$, HEK-AAV-$CD9_{GFP}$ (CD9) cells; WT, wild-type HEK-AAV cells.

$CD9_{GFP}$ Increases the Number of AAVs Associated with Exosomes

Demonstrating that exo-AAV1-$CD9_{GFP}$ is on average 26% more efficient than wild-type exo-AAV1, we reasoned that the increased exosome production induced by $CD9_{GFP}$ overexpression could increase the number of AAVs associated to exosomes.

To elucidate whether the higher efficiency of the exo-AAV1-$CD9_{GFP}$ (100,000 × *g* fractions) is the result of the increased amount of exosome-bound AAVs or improved performance of the exo-AAVs, we subjected the 100,000 × *g* pellet to a discontinuous iodixanol gradient to better separate exosome-bound AAVs and free AAVs.[17] As a control of the migration of free AAVs, we also subjected standard AAVs to the gradient (Figure 4A). The vector genomes were detected by real-time qPCR, and the percentage of total genomic copies per fraction was plotted (Figure 4B).

We detected vector genomes in all fractions and determined different distributions between the samples (wild-type [WT], $CD9_{GFP}$, and standard AAV). We found standard AAV1 located mainly in fractions 14–18 (98.5%), confirming the expected distribution of free AAVs. Finding that the exosomes were mainly distributed up to fraction 6, this allowed us to classify the lower density fractions, according to our finding and the literature,[17,24] as vesicle-bound AAVs. Knowing from the western blots that our input material is from exosomal origin and as an additional control, we analyzed in a more sensitive assay the distribution of exosomes of the 100,000 × *g* pellets of wild-type and $CD9_{GFP}$-overexpressing cells on the gradient by determining the acetylcholinesterase (AChE) activity of each fraction (Figure 4D), which is another marker protein of exosomes.

As expected, we found numerous vector genomes in the low-density fractions (4–13) of both 100,000 × *g* pellets ($CD9_{GFP}$ and WT; Figures 4A and 4B). All samples sedimented with less than 1% in fractions 1–3.

For a better evaluation, we separated the iodixanol gradient into two categories: free AAVs in high iodixanol density (14–18) and exosome-associated AAVs in low-density fractions (4–13; Figures 4A and 4C). We observed that 29.95% of exo-AAV1 is recovered in exosome density fractions, whereas it increased to 47.66% for exo-AAV1-$CD9_{GFP}$ (Figure 4C). These results suggest that the higher exo-AAV1-$CD9_{GFP}$ transduction efficiency is the result of an increment of AAVs associated with membranous vesicles.

DISCUSSION

Exosome-associated AAVs (exo-AAVs) hold advantages over standard AAVs because they have increased resistance to antibodies and higher transduction efficiency and the membrane can be

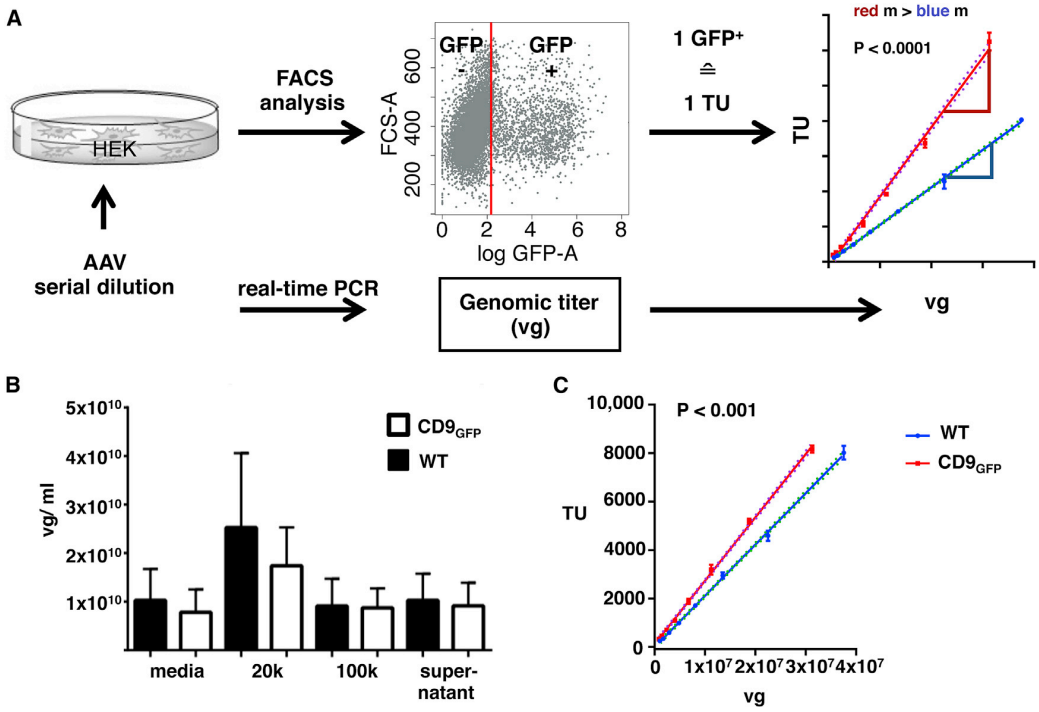

Figure 3. exo-AAV1-CD9$_{GFP}$ Had Enhanced Transduction Efficiency

(A) Method diagram illustrating the titration process of rAAVs. HEK cells were transduced with a serial dilution of AAV samples with defined genomic titer. The percentage of transduced cells was determined by FACS analysis. One GFP$^+$ cell thereby equals one transducing unit (TU), which was plotted over the vector genomes (vg). A linear regression line was fitted in the data points of three experimental rounds. The slopes of the linear regression lines (m) from two different samples (hypothetical "red" and "blue") were tested for a significant difference (two-tailed p value). The quotient of needed vector genomes to have one transducing unit (vg/TU) gives the efficiency of the virus, with a lower quotient being better. (B) In each exo-AAV1 harvesting step, the genomic titer was in an unpaired t test not significantly different for wild-type and overexpression cell line. Error bars indicate the SD of biological triplicates determined by real-time PCR measurements. (C) HEK cells were transduced with a dilution series of 100,000 pelleted viruses, and the amount of transducing units were calculated by the number of GFP-expressing cells. Exo-AAV1-CD9$_{GFP}$ was in mean 26% more efficient when considering three rounds of production. Error bars indicate the SD of technical triplicates. Linear regression was used to test slopes (m) with a two-tailed p value for a significant difference (indicated in the graph). CD9$_{GFP}$, exo-AAVs from HEK-AAV-CD9$_{GFP}$ (CD9) cells; WT, exo-AAVs from wild-type HEK-AAV cells.

modified to increase target specificity.[14,17] Because any improvement in AAV production will be remarkably exciting and essential for the future of gene therapy, we examined (as proof of concept) how an enhanced exosome production influences the release and efficiency of recombinant exo-AAVs.

We described previously that the exogenous expression of the tetraspanin CD9 increases exosome production in several cell lines.[23] In this study, we generated HEK-AAV cells expressing CD9$_{GFP}$ and demonstrated that exo-AAV1-CD9$_{GFP}$ from these cells had an increased transduction efficiency of 26% ± 4.9% (mean ± SD) compared to conventional exo-AAV1. Furthermore, we showed that the increased transduction efficiency is most likely due to a higher yield of exosome-bound AAVs.

An increase of exosome production was achieved by transduced HEK-AAV cells with a lentivirus to express a GFP-fused version of the tetraspanin CD9. First, secreted vesicles were extracted as previously performed using PEG precipitation,[23] and second, we introduced the ultracentrifugation purification protocol used for exo-AAV harvesting and confirmed our data. We confirmed the existence of exosomal markers and especially the CD9$_{GFP}$ fusion protein in the exo-AAV preparation by the detection of several exosomal marker proteins. More interestingly, CD9$_{GFP}$ was only and in a high amount detected in samples from the overexpressing cell line, which additionally to the flow cytometry analysis prior to virus production shows the strong overexpression of CD9$_{GFP}$. We suggest that the amount of native CD9 in the PEG-precipitated sample remained below the detection limit.

Because AAV production does not enhance microvesicle release,[14] we assumed the same vesicle distribution during AAV1 production. To keep the exosome characterization close to AAV1 production conditions, the control cells were transfected with pAAV-CAG-GFP without the helper plasmid. The analysis of the vesicle size and concentration from NTA measurements showed that CD9$_{GFP}$

Table 1. Total Yield of Vector Genomes per Plate (Mean ± SD)

	HEK-AAV	HEK-AAV-CD9$_{GFP}$
Media	$1.03 \times 10^{11} \pm 7.3 \times 10^{10}$	$7.8 \times 10^{10} \pm 5.09 \times 10^{10}$
100,000 × *g* pellet	$5.2 \times 10^{8} \pm 3.7 \times 10^{8}$	$5 \times 10^{8} \pm 2.5 \times 10^{8}$
Standard AAV	–	$8.08 \times 10^{10} \pm 8 \times 10^{9}$

Media and 100,000 × *g* pellet from biological triplicates were measured in technical triplicates. Standard AAVs isolated from the crude lysate were measured in technical triplicates.

overexpression increases the exosome concentration of vesicles precipitated by PEG as well as in the 100,000 × *g* pellet. These findings indicate that the overexpression is indeed increasing the exosome output and does not reflect an artifact of the PEG precipitation.

Analyzing the genomic titer of the exo-AAV harvesting steps (media, 20,000 × *g*, 100,000 × *g*, and supernatant), we observed no significant differences between wild-type and CD9$_{GFP}$-overexpressing cells for viral particle production. But we found in iodixanol gradient analysis that, upon CD9$_{GFP}$ overexpression, the number of AAVs associated to exosomes increases. We presume that this is the reason for the enhanced transduction efficiency of exo-AAV1-CD9$_{GFP}$. In the AChE enzyme assays of exosomes derived from the wild-type and the CD9-overexpressing cells, we observed approximately very similar activities in all expected exosome-positive gradient fractions. Thus, we can conclude that the amount of secreted exosomes was increased upon CD9$_{GFP}$ overexpression, whereas the overall concentration of AchE remained on a constant level. This is another interesting finding for the future work on the influence of enhanced exosome production and the protein content of such vesicles.

On the gradient, we observed a similar distribution of free and vesicle-associated viruses as reported before for AAVs and other viruses, like HIV and hepatitis C.[17,23–25]

Recent studies revealed that non-enveloped viruses, like hepatitis, are co-released by the cellular exosomal pathway and occur in a quasi-enveloped form (membrane associated with viral glycoproteins).[26] These results suggested that exosome association is not exclusive for AAV or induced by the experimental setup. Moreover, experiments on exosome-associated hepatitis E virus showed that, upon bafilomycin A1 treatment,[27] a lysosomal inhibitor, the production of exosomes increases.[28] Thereby, the number of virus in the media rises, whereas the knockdown of the exosome machinery induced a reduction of virus in the media.[27] These findings imply that the modulation of the exosome pathway can be used to manipulate the production of exosome-associated viruses and that this route is also taken by viruses in their native host cells.[29,30] Here, we show that this holds true for AAV1 and that probably a combined approach of bafilomycin A1 treatment and CD9$_{GFP}$ overexpression could further improve the exo-AAV engineering. For detailed analysis of biophysical properties of CD9-enriched vesicles, we suggest more experiments to elucidate whether the CD9$_{GFP}$ stabilizes membranes, enables interaction with the AAV capsid, or supports the fusion with the recipient cell.

More efficient AAVs are required to decrease the high AAV doses needed for systemic delivery (10^{13} to 10^{14} vector genomes per kg of body weight)[31] to achieve a sufficient gene expression, e.g., in the CNS. Exo-AAVs are therefore a suitable tool, being more efficient to cross the blood-brain barrier than the standard AAVs and highly efficient in neuronal transduction.[18] Here, we demonstrate that, with minor adjustments in the production protocol in a CD9-enriched system, it is possible to increase both exo-AAV yield and efficiency by about 26%.

We consider this work as a proof of principle and therefore used our standard AAV production protocols using HEK-AAV cells, i.e., E1-transformed HEK293 in a helper-free system. This required the transduction of early passaged HEK-AAV cells (passage five) without leaving sufficient time for full selection of CD9$_{GFP}^{+}$ cells. This was to avoid reduction of the E1 expression that is commonly seen after several passages. For the future, we consider generating a HEK-AAV cell line with a stable and homogeneous expression of both E1 and CD9 to increase the exo-AAV production under standard conditions.

In conclusion, CD9$_{GFP}$ overexpression in HEK-AAV producer cells enhances the efficiency of exo-AAV1 by raising the association of the AAVs with the exosomes, leading to a better viral genome to transducing unit ratio.

MATERIALS AND METHODS

Cell Culture

Cells were split twice a week and cultivated at 37°C with 5% CO_2 in a humidified atmosphere. HEK was kept in DMEM (GIBCO, Life Technology, Darmstadt, Germany), supplemented with penicillin/streptomycin (100 units/mL; 0.1 mg/mL) and 10% fetal calf serum (FCS) (GIBCO, Life Technology, Darmstadt, Germany). HEK-AAV cells (Agilent Technologies, CA) were kept in DMEM, supplemented with penicillin/streptomycin (100 units/mL; 0.1 mg/mL), 15% FCS, 1 mM sodium pyruvate, and 1 mM L-glutamine. The stable HEK293FT-CD9$_{GFP}$ cell line was generated as described previously.[23] In brief, cells were seeded in 24-well plates and infected with lentiviruses carrying the VSVG envelope glycoproteins and containing CD9$_{GFP}$ as gene of interest. Successfully transduced cells were selected with blasticidin. Recombinant HEK-AAV-CD9$_{GFP}$ cells were gained by transfection with the lentivirus LV-CD9$_{GFP}$-VSV-G and not further selected with antibiotics but monitored by flow cytometry for GFP-expression and used for rAAV production when at least 80% of the cells expressed the transgene.

Generation of Lentiviral Constructs and Production

The CD9$_{GFP}$ fusion protein was cloned as previously described[23] from mEmerald-CD9-10 (Addgene plasmid no. 54029, a gift from Michael Davidson) into the pENTR1a no CCDB. Gateway cloning with LR

Table 2. Ratio of Vector Genomes per Transducing Units in 100,000 × *g* and Media

	vg/TU		
Fraction	exo-AAV1	exo-AAV-$CD9_{GFP}$	% exo-AAV-$CD9_{GFP}$ Efficiency
100,000 × *g* pellet	1,131	838	+26
	2,894	1,968	+32
	4,699	3,743	+20
Media	811	759	+6
	3,102	2,851	+8

reaction was performed according to manufacturer's condition using pLENTI6.3/TO/V5-Dest as destination vector (Thermo Fisher Scientific, Waltham, MA, USA). $CD9_{GFP}$ pseudotyped lentiviruses were produced in HEK293FT cells. These were seeded in two T75 flasks at 8.25 × 10^5 cells/mL and directly transfected with pLenti-$CD9_{GFP}$ for gene of interest (GOI) delivery, psPAX2 (Addgene plasmid no. 12260, a gift from Didier Trono) for viral capsid proteins, and pCMV-VSV-G (Addgene plasmid no. 8454, a gift from Bob Weinberg)[32] for viral envelope proteins. 16 hr after transfection, sodium-butyrate-containing media (0.01 M) was added for 8 hr. Afterward, media without sodium butyrate was used and collected every 24 hr. After 5 days, media was centrifuged 30 min at 2,000 × *g*, filtered (450 μm), and stored at −80°C.

Virus Production and Isolation

AAV2/1-CAG-GFP was produced in HEK-AAV cells seeded in 15-cm dishes 48 hr prior to transfection. Calcium phosphate transfection was performed in DMEM-F12 (GIBCO, Life Technology, Darmstadt, Germany) with penicillin/streptomycin and 2% FCS. Per plate, 73.6 μg pDP1rs (Plasmid Factory, Bielefeld, Germany) and 18.4 μg pAAV-CAG-GFP carrying ITRs of AAV2 (Addgene plasmid no. 28014, a gift from Karel Svoboda) were applied. After 8 hr, the media was changed to DMEM, supplemented with penicillin/streptomycin, 2% FCS, 1 mM sodium pyruvate, and 1 mM L-glutamine. For the mimicked AAV production, we transfected only the pAAV-CAG-GFP.

The next day, media was changed to 10 mL DMEM, supplemented with penicillin/streptomycin, 1 mM sodium pyruvate, 1 mM L-glutamine, and 2% exosome-free FCS (16 hr at 100,000 × *g* depleted FCS), and cells were cultivated for two days.

Harvest of exo-AAVs

The production and harvesting protocol of exo-AAVs was adapted from György et al.[17] In brief, exo-AAV1 was harvested from media of four plates, which was depleted at 300 × *g* for 5 min and 1,000 × *g* for 10 min. The supernatant was centrifuged at 20,000 × *g* in JS24.38 rotor (Beckman Coulter Genomics, Brea, CA) for 1 hr at 15°C. The pellet was resuspended in 200 μL DMEM, and the supernatant was centrifuged again at 100,000 × *g* for 1.5 hr at 15°C and the pellet as well resuspended (exo-AAV). Samples were kept at 4°C.

Harvest of Standard AAVs

The harvest of standard AAVs was performed according to Zolotukhin et al.[9] In brief, cells were resuspended in gradient buffer (100 mM Tris, 500 mM NaCl, and 100 mM $MgCl_2$) and, after one freeze/thaw cycle at −140°C/55°C, transferred through a 26G needle, followed by three freeze/thaw cycles. Free DNA was digested at 37°C for 1 hr with 500 U Benzonase per mL cell lysate. Cell debris was pelleted by centrifugation at 3,000 × *g* for 15 min and the supernatant loaded on an iodixanol density gradient (15%, 25%, 40%, and 60% iodixanol diluted in gradient buffer). The gradient was centrifuged at 103,000 × *g* for 15 hr at 4°C, and the 40% fraction was harvested. The buffer was exchanged during dialysis to PBS, supplemented with 0.05 mM $MgCl_2$ and 0.395 mM KCl in 100,000 Da MWCO dialyse membrane (Roth, Karlsruhe, Germany). The virus was concentrated in ViVAspin 20 concentrator (Rettberg, Göttingen, Germany) with 100,000 Da MWCO.

Vector Genome Quantification

Genomic AAV titer was determined with modifications according to Rohr et al.[33] by real-time qPCR with SensiMix SYBR Hi-ROX Kit (Bioline, London, UK) and primers that amplify the Woodchuck hepatitis virus posttranscriptional regulatory element (WPRE) region (reverse 5′- CCGAAGGGACGTAGCAGAAG-3′ and forward 5′-CTTGCCCGCTGCTGGAC-3′; Sigma-Aldrich, St. Louis, Missouri) according to the manufacturer's protocol.

A standard curve was run from an AAV plasmid of known concentration, and the virus titer was calculated accordingly. Each sample was measured in triplicates and the mean value plotted. Real-time PCR was performed with StepOnePlus Real-Time PCR System and related software (Thermo Fisher Scientific, Germany).

FACS Analysis

For FACS analysis, cells were trypsinized, pelleted at 300 × *g*, and washed three times with PBS. Cells were analyzed with the BD LSR II system (BD Biosciences, Franklin Lanes, NJ), the 505LP-BP530/30 filter set for GFP detection, and the FACSdiva software. The data were analyzed with Flowing Software.

Functional Virus Quantification

The transducing units (TUs) of AAV1 were determined by a transduction assay modified from Kutner et al.[34] HEK cells were seeded in 24-well plates and transfected at the next day with a 2:5 serial dilution of the virus in OptiMEM (GIBCO, Life Technology, Darmstadt, Germany) supplemented with 2% XerumFree (TNCBio, Eindhoven, Netherlands). Cells were harvested 48 hr after transduction, prepared, and analyzed by FACS analysis. The percentage of GFP-positive cells was used to calculate the total amount of transduced cells. The amount of GFP-expressing cells as TUs was plotted against the genome copies per well, and a linear regression was applied. The TUs/vg is given by the y value for 1 vector genome.

PEG Precipitation of Vesicles

Vesicle-containing media was depleted at 500 × *g* for 5 min and at 2,000 × *g* for 30 min. The supernatant was filtered through 0.45-μm

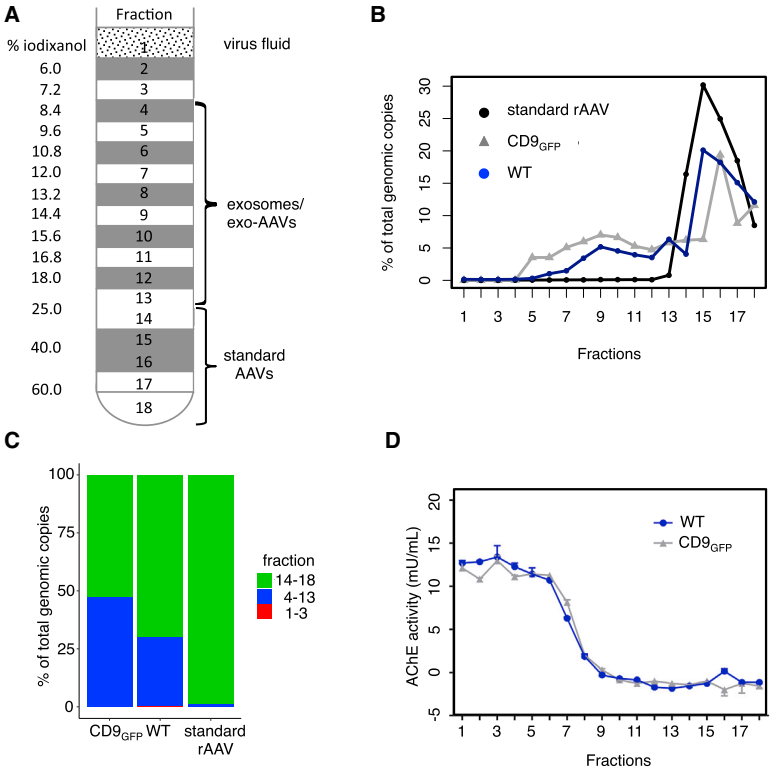

Figure 4. exo-AAV-CD9$_{GFP}$ Enriched in Lower Iodixanol Density Fractions

(A) Standard AAV1, exo-AAV1, and exoAAV1-CD9$_{GFP}$ were applied on an iodixanol density gradient to separate exosome-bound AAVs from free AAVs. (B and C) Standard AAV1 accumulated with 98.5% in fractions 14–18, whereas exo-AAV1 migrated with 29.25% in fractions 4–13 and exo-AAV1-CD9$_{GFP}$ with 47.66%. For all, less than 1% was collected in fractions 1–3. (D) Acetylcholinesterase (AchE) activity of iodixanol density gradient fractions of wild-type HEK and HEK-CD9$_{GFP}$ 100,000 × *g* pellets. The mean of technical duplicates with range is plotted.

filter device and mixed with 16.6% PEG (1:5 PEG8000 in PBS). The mixture was incubated under constant rotation at 4°C for 16 hr and vesicles isolated by centrifugation at 1,500 × *g* for 30 min. The pellet was resuspended in PBS or DMEM as previously described.[35]

Nanoparticle Tracking Analysis

Extracellular vesicles were analyzed with the NanoSight LM10 instrument (Malvern Instruments, Worcestershire, UK) with a recording time of 30 s. The data were processed with NTA software 2.3.[36]

Analytical Gradient Centrifugation

Standard AAVs and exo-AAVs were separated on an analytical discontinuous iodixanol gradient with 14 fractions of increasing iodixanol concentration (see Figure 4) in PBS (with modifications from Dettenhofer and Yu[37]). The virus was applied in DMEM and the gradient centrifuged for 16 hr at 4°C and 103,000 × *g*. The gradient was harvested in 18 fractions of 1 mL from top to bottom.

Acetylcholinesterase Activity Detection Assay

Acetylcholinesterase activity was measured using the Amplite Colorimetric Acetylcholinesterase Assay Kit (AAT Bioquest, Sunnyvale, CA, USA) according to the manufacturer's instructions. In brief, samples were incubated with acetylcholinesterase substrate on a 96-well plate. Absorbances were measured at 410 nm on a Synergy 2 Multi-detection Microplate Reader (Biotek Instruments, Winooski, VT, USA). The acetylcholinesterase activity was calculated in mU/mL using linear regression.

Western Blot Analysis

The protein samples were incubated with RIPA buffer (10×) and TCA precipitated, and the dried pellet was dissolved in Laemmli buffer. Equal volumes were loaded on an SDS-PAGE, separated, and transferred on a nitrocellulose membrane. The membrane was blocked by NETT-G (1.5 M NaCl, 0.05 M EDTA, 0.5 M Tris, 0.5% Triton X-100, and 0.25% gelatine; incubated with the primary antibody overnight [anti-CD9 1:500 (ab92726; Abcam, USA), anti-CD63 1:1,000 (10628D; Thermo Fisher Scientific, CA, USA), anti-Alix 1:1,000 (634502; BioLegend, CA, USA), anti-GFP 1:500 (ab38689; Abcam, USA), and anti-AAV 1:1,000 (60158; PROGEN Biotechnik, Heidelberg, GE)] and with the secondary antibody for 2 hr [horseradish peroxidase (HRP)-coupled goat anti-mouse secondary antibody 1:10,000 (Life Technologies) and anti-rabbit 1:10,000 (G-21234; Life Technologies, CA, USA)]). The membrane was incubated with horseradish peroxidase substrate (Luminata Forte, Merck, Germany), and the chemiluminescence was detected by an ECL machine (Chemocam Imager, INTAS, Germany).

Microscopy

Phase and fluorescence microscopy pictures were taken 72 hr post-transduction with LV-CD9$_{GFP}$-VSV-G at the Axio Vert.A1 (Carl Zeiss, Göttingen, Germany) with the filter set P 525/50 (GFP/YFP).

Statistics and Software

Statistics and graphical presentations were done with GraphPad Prism6 or R, as illustrations were done with ChemDraw Professional 15.1.

SUPPLEMENTAL INFORMATION

Supplemental Information includes two figures and can be found with this article online at https://doi.org/10.1016/j.omtm.2018.03.008.

AUTHOR CONTRIBUTIONS

L.T.S. conducted the rAAV experiments. L.T.S., N.L.-D., and R.R.F. analyzed the data. L.T.S. and N.L.-D. performed the western blot

experiment. R.R.F. performed cell cultivation and the acetylcholinesterase assay. K.O.B. and R.R.F. provided the lentivirus. K.O.B. gave technical assistance for the NTA data acquisition and plotting. L.T.S., N.L.-D., and J.G. conceived and designed the study. L.T.S., N.L.-D., and J.G. wrote the manuscript.

ACKNOWLEDGMENTS

We thank Dr. S. Schneider for comments on the manuscript and help with data analysis, A. Backhaus and A. Schuder for expert technical assistance, and Dr. Vladan Rankovic and Prof. Dr. Tobias Moser for providing the GFP antibody. We thank Prof. A. Schneider and Dr. M. Kunadt for providing the NTA machine and technical support. This work was partly supported by the Göttingen Graduate School for Neuroscience, Biophysics, and Molecular Biosciences (DFG grant GSC 226/2), the LifeScience Stiftung (DPZ 2014.01), and the CNPq (grant CNPq234389/2014-1).

REFERENCES

1. Kay, M.A. (2011). State-of-the-art gene-based therapies: the road ahead. Nat. Rev. Genet. *12*, 316–328.
2. Mingozzi, F., and High, K.A. (2013). Immune responses to AAV vectors: overcoming barriers to successful gene therapy. Blood *122*, 23–36.
3. Daya, S., Cortez, N., and Berns, K.I. (2009). Adeno-associated virus site-specific integration is mediated by proteins of the nonhomologous end-joining pathway. J. Virol. *83*, 11655–11664.
4. Hocquemiller, M., Giersch, L., Audrain, M., Parker, S., and Cartier, N. (2016). Adeno-associated virus-based gene therapy for CNS diseases. Hum. Gene Ther. *27*, 478–496.
5. Keeler, A.M., ElMallah, M.K., and Flotte, T.R. (2017). Gene therapy 2017: progress and future directions. Clin. Transl. Sci. *10*, 242–248.
6. Vandenberghe, L.H., Xiao, R., Lock, M., Lin, J., Korn, M., and Wilson, J.M. (2010). Efficient serotype-dependent release of functional vector into the culture medium during adeno-associated virus manufacturing. Hum. Gene Ther. *21*, 1251–1257.
7. Smith, R.H., Ding, C., and Kotin, R.M. (2003). Serum-free production and column purification of adeno-associated virus type 5. J. Virol. Methods *114*, 115–124.
8. Strobel, B., Miller, F.D., Rist, W., and Lamla, T. (2015). Comparative analysis of cesium chloride- and iodixanol-based purification of recombinant adeno-associated viral vectors for preclinical applications. Hum. Gene Ther. Methods *26*, 147–157.
9. Zolotukhin, S., Byrne, B.J., Mason, E., Zolotukhin, I., Potter, M., Chesnut, K., Summerford, C., Samulski, R.J., and Muzyczka, N. (1999). Recombinant adeno-associated virus purification using novel methods improves infectious titer and yield. Gene Ther. *6*, 973–985.
10. Théry, C., Zitvogel, L., and Amigorena, S. (2002). Exosomes: composition, biogenesis and function. Nat. Rev. Immunol. *2*, 569–579.
11. Chiba, M., Kimura, M., and Asari, S. (2012). Exosomes secreted from human colorectal cancer cell lines contain mRNAs, microRNAs and natural antisense RNAs, that can transfer into the human hepatoma HepG2 and lung cancer A549 cell lines. Oncol. Rep. *28*, 1551–1558.
12. Cheng, L., Sun, X., Scicluna, B.J., Coleman, B.M., and Hill, A.F. (2014). Characterization and deep sequencing analysis of exosomal and non-exosomal miRNA in human urine. Kidney Int. *86*, 433–444.
13. Kalluri, R., and LeBleu, V.S. (2016). Discovery of double-stranded genomic DNA in circulating exosomes. Cold Spring Harb. Symp. Quant. Biol. *81*, 275–280.
14. Maguire, C.A., Balaj, L., Sivaraman, S., Crommentuijn, M.H., Ericsson, M., Mincheva-Nilsson, L., Baranov, V., Gianni, D., Tannous, B.A., Sena-Esteves, M., et al. (2012). Microvesicle-associated AAV vector as a novel gene delivery system. Mol. Ther. *20*, 960–971.
15. Calcedo, R., Franco, J., Qin, Q., Richardson, D.W., Mason, J.B., Boyd, S., and Wilson, J.M. (2015). Preexisting neutralizing antibodies to adeno-associated virus capsids in large animals other than monkeys may confound in vivo gene therapy studies. Hum. Gene Ther. Methods *26*, 103–105.
16. Greenberg, B., Butler, J., Felker, G.M., Ponikowski, P., Voors, A.A., Pogoda, J.M., Provost, R., Guerrero, J., Hajjar, R.J., and Zsebo, K.M. (2016). Prevalence of AAV1 neutralizing antibodies and consequences for a clinical trial of gene transfer for advanced heart failure. Gene Ther. *23*, 313–319.
17. György, B., Fitzpatrick, Z., Crommentuijn, M.H., Mu, D., and Maguire, C.A. (2014). Naturally enveloped AAV vectors for shielding neutralizing antibodies and robust gene delivery in vivo. Biomaterials *35*, 7598–7609.
18. Hudry, E., Martin, C., Gandhi, S., György, B., Scheffer, D.I., Mu, D., Merkel, S.F., Mingozzi, F., Fitzpatrick, Z., Dimant, H., et al. (2016). Exosome-associated AAV vector as a robust and convenient neuroscience tool. Gene Ther. *23*, 380–392.
19. Wassmer, S.J., Carvalho, L.S., György, B., Vandenberghe, L.H., and Maguire, C.A. (2017). Exosome-associated AAV2 vector mediates robust gene delivery into the murine retina upon intravitreal injection. Sci. Rep. *7*, 45329.
20. György, B., Sage, C., Indzhykulian, A.A., Scheffer, D.I., Brisson, A.R., Tan, S., Wu, X., Volak, A., Mu, D., Tamvakologos, P.I., et al. (2017). Rescue of hearing by gene delivery to inner-ear hair cells using exosome-associated AAV. Mol. Ther. *25*, 379–391.
21. Hemler, M.E. (2005). Tetraspanin functions and associated microdomains. Nat. Rev. Mol. Cell Biol. *6*, 801–811.
22. Böker, K.O. (2017). Functional characterization of npcRNAs: intercellular trafficking of generegulatory components via exosomes. PhD thesis (University of Göttingen).
23. Böker, K.O., Lemus-Diaz, N., Rinaldi Ferreira, R., Schiller, L., Schneider, S., and Gruber, J. (2018). The impact of the CD9 tetraspanin on lentivirus infectivity and exosome secretion. Mol. Ther. *26*, 634–647.
24. Cantin, R., Diou, J., Bélanger, D., Tremblay, A.M., and Gilbert, C. (2008). Discrimination between exosomes and HIV-1: purification of both vesicles from cell-free supernatants. J. Immunol. Methods *338*, 21–30.
25. Liu, Z., Zhang, X., Yu, Q., and He, J.J. (2014). Exosome-associated hepatitis C virus in cell cultures and patient plasma. Biochem. Biophys. Res. Commun. *455*, 218–222.
26. Nagashima, S., Takahashi, M., Kobayashi, T., Tanggis, Nishizawa, T., Nishiyama, T., Primadharsini, P.P., and Okamoto, H. (2017). Characterization of the quasi-enveloped hepatitis E virus particles released by the cellular exosomal pathway. J. Virol. *91*, e00822-17.
27. Nagashima, S., Jirintai, S., Takahashi, M., Kobayashi, T., Tanggis, Nishizawa, T., Kouki, T., Yashiro, T., and Okamoto, H. (2014). Hepatitis E virus egress depends on the exosomal pathway, with secretory exosomes derived from multivesicular bodies. J. Gen. Virol. *95*, 2166–2175.
28. Alvarez-Erviti, L., Seow, Y., Schapira, A.H., Gardiner, C., Sargent, I.L., Wood, M.J., and Cooper, J.M. (2011). Lysosomal dysfunction increases exosome-mediated alpha-synuclein release and transmission. Neurobiol. Dis. *42*, 360–367.
29. Feng, Z., Hirai-Yuki, A., McKnight, K.L., and Lemon, S.M. (2014). Naked viruses that aren't always naked: quasi-enveloped agents of acute hepatitis. Annu. Rev. Virol. *1*, 539–560.
30. Lemon, S.M., and Binn, L.N. (1985). Incomplete neutralization of hepatitis A virus in vitro due to lipid-associated virions. J. Gen. Virol. *66*, 2501–2505.
31. György, B., and Maguire, C.A. (2017). Extracellular vesicles: nature's nanoparticles for improving gene transfer with adeno-associated virus vectors. Wiley Interdiscip. Rev. Nanomed. Nanobiotechnol., Published online August 11, 2017. https://doi.org/10.1002/wnan.1488.
32. Stewart, S.A., Dykxhoorn, D.M., Palliser, D., Mizuno, H., Yu, E.Y., An, D.S., Sabatini, D.M., Chen, I.S., Hahn, W.C., Sharp, P.A., et al. (2003). Lentivirus-delivered stable gene silencing by RNAi in primary cells. RNA *9*, 493–501.

33. Rohr, U.P., Wulf, M.A., Stahn, S., Steidl, U., Haas, R., and Kronenwett, R. (2002). Fast and reliable titration of recombinant adeno-associated virus type-2 using quantitative real-time PCR. J. Virol. Methods *106*, 81–88.

34. Kutner, R.H., Zhang, X.Y., and Reiser, J. (2009). Production, concentration and titration of pseudotyped HIV-1-based lentiviral vectors. Nat. Protoc. *4*, 495–505.

35. Alvarez, M.L., Khosroheidari, M., Kanchi Ravi, R., and DiStefano, J.K. (2012). Comparison of protein, microRNA, and mRNA yields using different methods of urinary exosome isolation for the discovery of kidney disease biomarkers. Kidney Int. *82*, 1024–1032.

36. Dragovic, R.A., Gardiner, C., Brooks, A.S., Tannetta, D.S., Ferguson, D.J., Hole, P., Carr, B., Redman, C.W., Harris, A.L., Dobson, P.J., et al. (2011). Sizing and phenotyping of cellular vesicles using Nanoparticle Tracking Analysis. Nanomedicine (Lond.) *7*, 780–788.

37. Dettenhofer, M., and Yu, X.F. (1999). Highly purified human immunodeficiency virus type 1 reveals a virtual absence of Vif in virions. J. Virol. *73*, 1460–1467.